Rapid Near-Optimal Aerospace Plane Trajectory Generation and Guidance

J. E. Corban,* A. J. Calise,† and G. A. Flandro†
Georgia Institute of Technology, Atlanta, Georgia 30332

Problems associated with onboard trajectory optimization, propulsion system cycle selection, and the synthesis of guidance laws are addressed for ascent to low Earth orbit of an airbreathing, single-stage-to-orbit vehicle. A multicycle propulsion system is assumed that incorporates turbojet, ramjet, scramjet, and rocket engines. An energy state approximation is applied to a singularly perturbed, four-state dynamic model for flight of a point mass over a spherical nonrotating Earth. An algorithm is then derived for generating both the fuel-optimal climb profile and the guidance commands required to follow that profile. In particular, analytic switching conditions are derived that, under appropriate assumptions, efficiently govern optimal transition from one propulsion cycle to another. The algorithm proves to be computationally efficient and suitable for real-time implementation. It will accommodate general functional dependence on angle of attack, a normal component of thrust, acceleration limits, and constraints on maximum dynamic pressure and maximum aerodynamic heating rate. The paper concludes with the presentation of representative numerical results that illustrate the nature of the fuel-optimal climb paths and the tracking performance of the guidance algorithm.

Nomenclature

C_1	= inequality constraint, dynamic pressure
C_2	= inequality constraint, aerodynamic heating
C_3	= inequality constraint, tangential acceleration
C_4	= inequality constraint, normal acceleration
C_D	= drag coefficient
C_L	= lift coefficient
c_j	= thrust specific fuel consumption for engine type j
D	= aerodynamic drag
E	= mass specific energy
F_C	= thrust component aligned with the velocity vector
F_S	= thrust component normal to the velocity vector
f	= total fuel flow rate
f_{max_i}	= total fuel flow rate for any number of independent engines of type i combined, with each operating at a stoichiometric fuel-to-air ratio
g	= acceleration due to gravity at mean sea level
H	= Hamiltonian function
h	= altitude, given by $r - r_E$
J	= performance index
L	= aerodynamic lift
M	= Mach number
m	= vehicle mass
n	= total number of different engine cycles employed
$n - p$	= number of engine types employed for which fuel flow rate varies in direct proportion to φ but thrust varies in a nonlinear fashion with φ
n_1	= component of acceleration aligned with the velocity vector
n_2	= component of acceleration normal to the velocity vector
p	= number of engine types employed that exhibit linear dependence of both fuel flow rate and thrust on η
Q	= aerodynamic heating rate per unit area
q	= dynamic pressure
r	= radial distance from the center of the Earth
r_E	= mean sea level

S_j	= switching function for bang-bang control of η_j
s	= aerodynamic reference area
T	= net thrust
T_k	= combined thrust of any number of independent engines of type k, $k = 1$ to p
t	= time
t_f	= final time
U	= pseudocontrol variable
V	= velocity
W	= vehicle weight, taken at mean sea level, mg
α	= angle of attack
γ	= flight-path angle
ϵ	= perturbation parameter, 0 or 1
ϵ_{Tk}	= angle between T_k and the body longitudinal axis
η_j	= throttle control, engine type j
λ_x	= costate, subscript denotes related state
μ	= gravitational constant for the Earth
π	= vector containing control for each engine type
ρ	= atmospheric density
σ	= bank angle
τ	= transformed time variable, t/ϵ
φ_i	= fuel equivalence ratio, engine type i

I. Introduction

EMERGING technology in many engineering fields, including hypersonic airbreathing propulsion, computational fluid dynamics, and high-temperature materials, may soon make possible a vehicle configuration that has been the subject of study for over four decades.[1] This vehicle concept is commonly referred to as an aerospace plane. Its development, in one version or another, is being pursued by a number of industrialized nations. The current U.S. concept consists of a single-stage vehicle propelled, for the most part, by airbreathing engines. Most notable among the airbreathing cycles to be employed is that of the supersonic combustion ramjet or "scramjet." This aircraft is to be fueled by liquid or slush hydrogen and will take off and land horizontally on conventional runways. Operational objectives of the current technology demonstration program include hypersonic cruise in the upper atmosphere for long durations and the ability to accelerate to orbital velocity. Potential missions for derivative vehicles include transportation to low Earth orbit, intercontinental passenger transportation, and a wide range of defense missions.

This paper considers the particular mission of single-stage-to-orbit. Here, the use of airbreathing hypersonic propulsion and technology for greatly reduced launch operations promises an order of magnitude reduction in the cost of placing payloads in low Earth orbit.[2,3] However, aerospace plane operations will have to approach those of modern commercial airlines in order to be cost effective. Guidance and control technology dependent on premission, ground-based trajectory optimization, typical of today's space launch industry, is inadequate for this task. Real-time, onboard trajectory optimization will be required.[4,5]

The state of the art in trajectory optimization for complex nonlinear systems consists of a number of well-developed numerical methods of solution. Unfortunately, these algorithms are poorly suited for onboard, real-time implementation. They are, in general, computationally intense, require an initial guess of the solution, and are lacking in global-convergence characteristics. Although some success in designing a reliable algorithm to numerically solve a two-point boundary-value problem in an onboard computer has been achieved for orbit transfer,[6] the diverse mission requirements and complex control structure of a general purpose aerospace plane will likely require that structured methods for order reduction be employed.

Energy state approximations and singular perturbation methods have been successfully employed to derive near-analytic trajectory optimization algorithms in the past. Near-optimal feedback guidance laws have also been obtained. The results prove suitable for onboard, real-time implementation and also contribute considerable insight into the nature of the optimal profiles and their relation to vehicle aerodynamic and propulsion characteristics. Early studies were devoted to fighter aircraft performance optimization.[7-9] However, many of the modeling approximations employed for analysis of subsonic and supersonic aircraft optimal trajectories are not valid for a vehicle with hypersonic cruise and orbital capabilities.

This paper presents an analysis of the problem of fuel-optimal ascent to low Earth orbit of an airbreathing, single-stage-to-orbit vehicle. Section II presents the singularly perturbed problem formulation. A generic multicycle propulsion system is defined that incorporates turbojet, ramjet, scramjet, and rocket engines. Inequality constraints on dynamic pressure, aerodynamic heating rate, and vehicle acceleration are also introduced. In Sec. III, an algorithm for generating fuel-optimal climb profiles is derived employing an energy state approximation. This algorithm results from application of the minimum principle to a low-order dynamic model that includes general functional dependence on angle of attack and a normal component of thrust. Analytic switching conditions are derived that, under appropriate assumptions, govern optimal transition from one propulsion cycle to another. These conditions prove quite valuable for improving the computational speed of the algorithm. The use of bank angle to modulate the magnitude of the vertical component of lift is also investigated in this section. Section IV provides an overview of the derivation of feedback guidance laws using the technique of feedback linearization on a stretched (boundary-layer) time scale. Section V provides a discussion of representative numerical results and details a correction procedure needed by the energy state approximation in certain speed regimes. Section VI completes the paper with conclusions.

II. General Problem Formulation

Consider atmospheric flight of a point mass over a spherical nonrotating Earth. The equations governing such flight can be reduced to a four-state model as follows:

$$\dot{E} = \frac{V(F_C - D)}{m} \tag{1}$$

$$\dot{m} = -f(r, E, \pi, \alpha) \tag{2}$$

$$\epsilon\dot{\gamma} = \frac{(F_S + L)\cos\sigma}{mV} - \frac{\mu\cos\gamma}{Vr^2} + \frac{V\cos\gamma}{r} \tag{3}$$

$$\epsilon\dot{r} = V\sin\gamma \tag{4}$$

The perturbation parameter ϵ, which has been artificially inserted, is nominally 1. It is assumed that the atmosphere is stationary and that the thrust vector lies in the vehicle's plane of symmetry. In Eq. (1), mass specific energy E is employed as a state variable in place of velocity V, where

$$E = V^2/2 - \mu/r \tag{5}$$

The reference point for zero gravitational potential is taken at a radial distance approaching infinity. The symbol V is to be taken as

$$V = [2(E + \mu/r)]^{1/2} \tag{6}$$

everywhere it appears in this analysis. Position and heading dynamics are decoupled from Eqs. (1-4) by the assumption of a nonrotating Earth and are not considered in this paper.

Aerodynamic drag of the vehicle is given by

$$D = qsC_D(r, E, \alpha) \tag{7}$$

where

$$q = \rho V^2/2$$

Aerodynamic lift at trim is given by

$$L = qsC_L(r, E, \alpha) \tag{8}$$

A multicycle propulsion system composed of n different engine cycles is assumed. Net thrust is given by

$$T = [F_C^2 + F_S^2]^{1/2} \tag{9}$$

F_C and F_S are depicted in Fig. 1 and are given by

$$F_C = \sum_{j=1}^{p} \eta_j T_j \cos(\alpha + \epsilon_{T_j}) + \sum_{i=p+1}^{n} T_i \cos(\alpha + \epsilon_{T_i}) \tag{10}$$

$$F_S = \sum_{j=1}^{p} \eta_j T_j \sin(\alpha + \epsilon_{T_j}) + \sum_{i=p+1}^{n} T_i \sin(\alpha + \epsilon_{T_i}) \tag{11}$$

Each of the n engine cycles (i.e., turbojet, ramjet, scramjet, rocket, etc.) is controlled by variation of the fuel flow rate in direct proportion to command. Of the total number of engine cycles to be considered, p are assumed to exhibit a linear relation between fuel flow rate and thrust generation. This assumption is typically employed for rocket engines. Each engine of this type carries an index j and shall be controlled by varying its throttle setting η_j. For the remaining $n-p$ engine cycles, the relation between fuel flow rate and thrust generation is assumed nonlinear. This behavior is typical of airbreathing cycles. Each engine of this type carries an index i and shall be controlled by variation in its fuel equivalence ratio φ_i.

The subscripted symbol T_k (where k represents either index j or i) in (10) and (11) represents the net thrust generated by any number of independent engines employing a particular
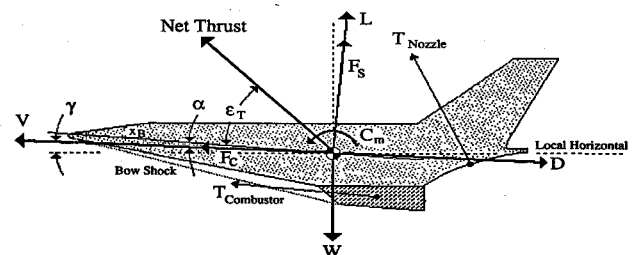

Fig. 1 Partial force and moment diagram.

cycle k. The symbol ϵ_{T_k} denotes the angle between T_k and the body longitudinal axis (see Fig. 1). Note that in general,

$$T_j = T_j(r,E,\alpha), \qquad \eta_j \in [0,1], \qquad j = 1 \text{ to } p \qquad (12)$$

$$T_i = T_i(r,E,\varphi_i,\alpha), \qquad \varphi_i \in [0,1], \qquad i = p + 1 \text{ to } n \qquad (13)$$

$$\epsilon_{T_k} = \epsilon_{T_k}(r,E,\alpha), \qquad k = 1 \text{ to } n \qquad (14)$$

The total fuel flow rate f is given by

$$f = \sum_{j=1}^{p} \eta_j\, c_j(r,E,\alpha)T_j(r,E,\alpha) + \sum_{i=p+1}^{n} \varphi_i\, f_{\max_i}(r,E,\alpha) \qquad (15)$$

where c_j represents the thrust specific fuel consumption for engine type j and $f_{\max_i}$ represents the product of thrust specific fuel consumption and thrust at a stoichiometric fuel-to-air ratio for engine type i. For convenience, all of the engine throttle controls are collected into a single vector as follows:

$$\pi^T = [\eta_1, \eta_2, \ldots, \eta_p, \varphi_{p+1}, \ldots, \varphi_n] \qquad (16)$$

The control variables are angle of attack α, bank angle σ, the engine throttle settings η_j, for engine types 1 through p,

and the fuel equivalence ratios φ_i, for engine types $p + 1$ through n. The objective is to minimize the fuel consumed in gaining a specified final value for specific energy, with the performance index given by

$$J = -m(t_f) \qquad (17)$$

The final time t_f is free. Minimization of Eq. (17) is to be carried out subject to maximum dynamic pressure and maximum aerodynamic heating rate inequality constraints and acceleration limits defined by

$$C_1(r,E) = q - q_{\max} \leq 0 \qquad (18)$$

$$C_2(r,E,\alpha) = Q - Q_{\max} \leq 0 \qquad (19)$$

$$C_3(r,E,m,\alpha,\pi) = n_1 - n_{1\max} \leq 0 \qquad (20)$$

$$C_4(r,E,m,\alpha,\pi) = n_2 - n_{2\max} \leq 0 \qquad (21)$$

The symbols n_1 and n_2 represent the accelerations in g along and normal to the velocity vector (i.e., in the lift direction), respectively.
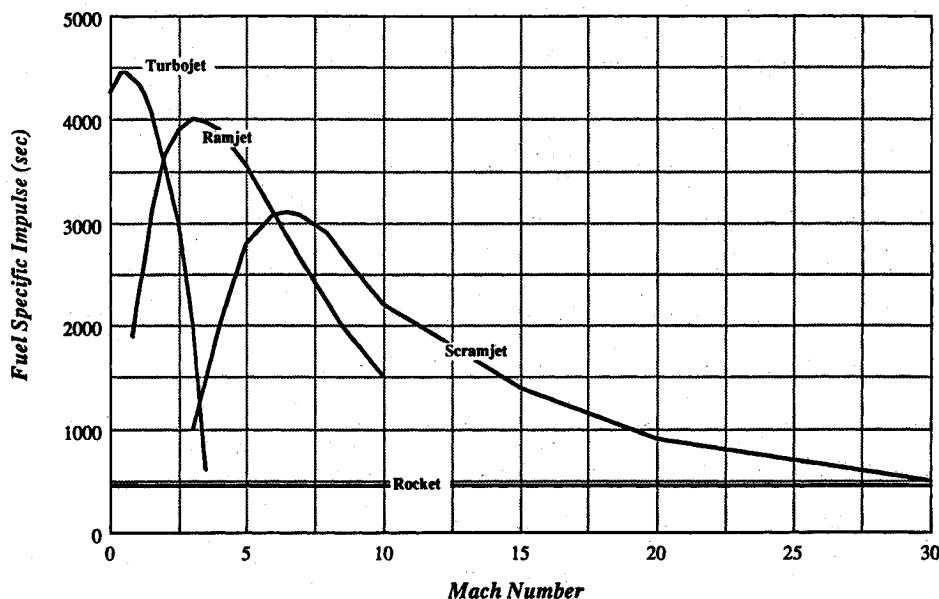

Fig. 2 Fuel specific impulse vs Mach number for the propulsion cycles used in vehicle models 2 and 3.
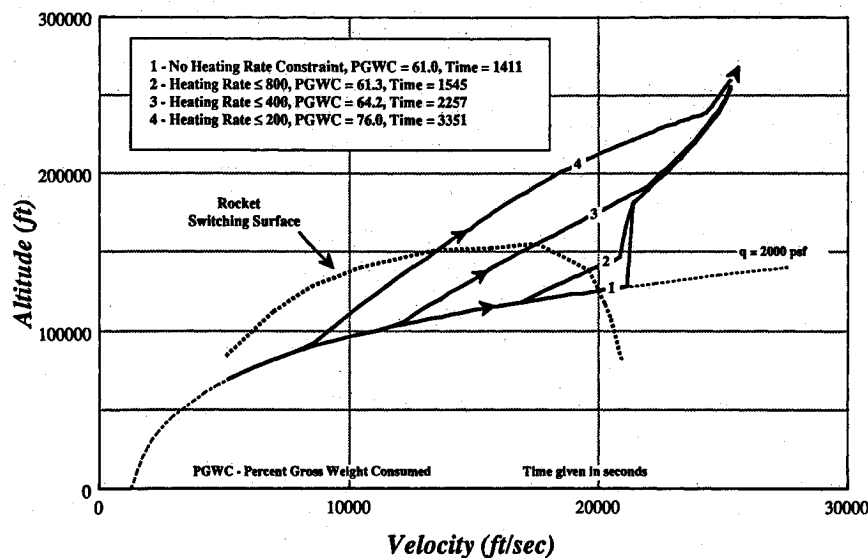

Fig. 3 Dependence of the reduced solution for vehicle model 1 on the aerodynamic heating rate constraint (W/cm²).

III.   Reduced Solution:
The Energy State Approximation

Simplified Analysis

We first consider a simplified problem in which flight is constrained to a vertical plane, the thrust vector is aligned with the velocity vector, and thrust production is assumed independent of vehicle angle of attack:

$$\sigma = 0, \qquad F_S = 0, \qquad F_C = T \qquad (22)$$

Furthermore, we consider only that portion of the trajectory in the hypersonic speed regime. In this regime, we need only consider a dual-cycle propulsion system (i.e., $n = 2$). The system consists of a bank of scramjet engine modules assumed to operate continuously at maximum throttle and a rocket engine that can be throttled as desired. In this simplified setting, the total fuel flow rate and net thrust can be respresented as

$$T = T_s(r,E) + \eta T_r(r), \qquad \eta \in [0,1] \qquad (23)$$

$$f = c_s(r,E)T_s + \eta c_r(r)T_r \qquad (24)$$

where thrust specific fuel consumption is represented by c_s for the scramjet and c_r for the rocket. Constraint (20), which can lead to the requirement for intermediate values of engine throttle settings, will be ignored.

Under these assumptions, the governing equations of motion can be written as

$$\dot{E} = \frac{V(T-D)}{m} \qquad (25)$$

$$\dot{m} = -f(r,E,\eta) \qquad (26)$$

$$\epsilon\dot{\gamma} = \frac{L}{mV} - \frac{\mu\cos\gamma}{Vr^2} + \frac{V\cos\gamma}{r} \qquad (27)$$

$$\epsilon\dot{r} = V\sin\gamma \qquad (28)$$

The control variables are now rocket engine throttle η and vehicle lift L. The objective remains to minimize the fuel consumed in gaining a specified final value of specific energy.
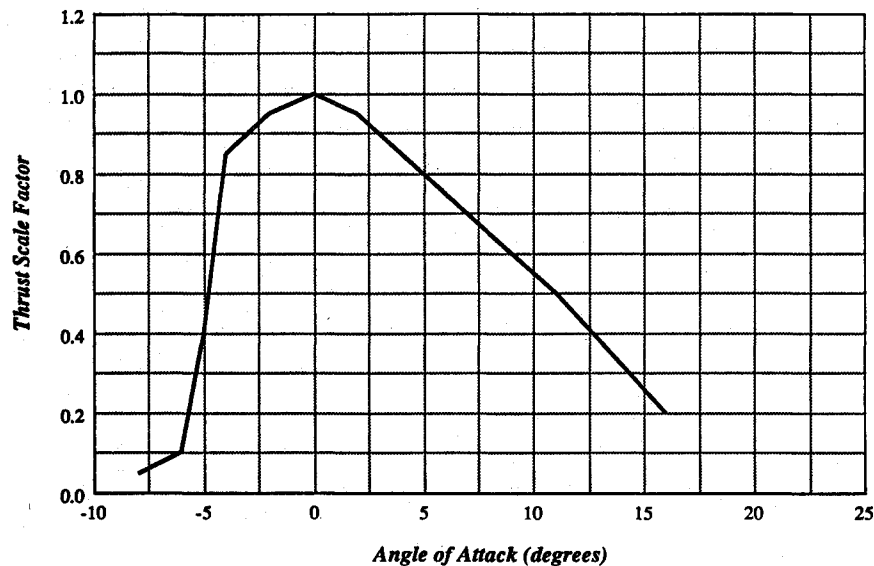

Fig. 4   Assumed variation in scramjet thrust with angle of attack.
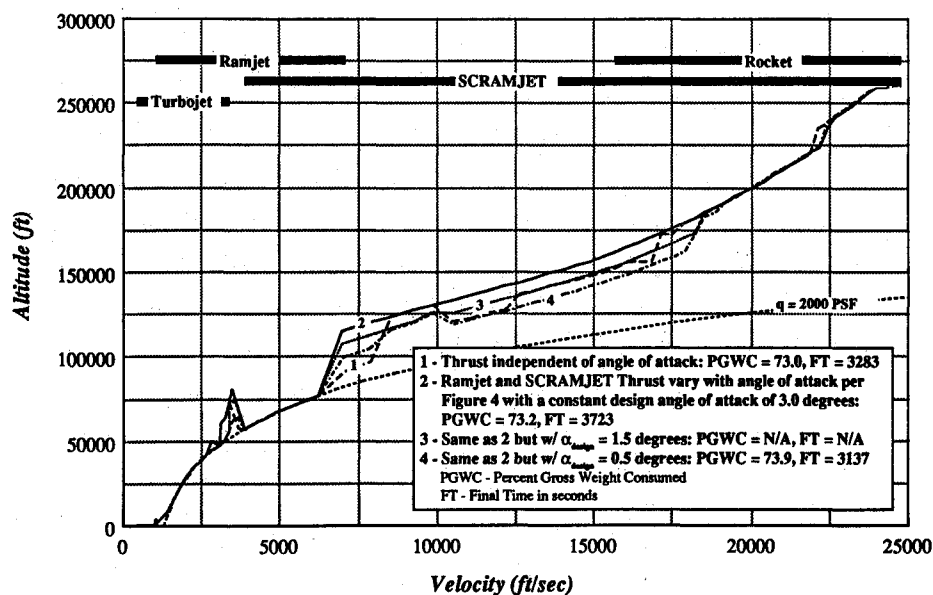

Fig. 5   Reduced solutions for vehicle model 2 as scramjet design angle of attack is varied.

Setting $\epsilon = 0$ in Eqs. (25-28) reduces the order of the dynamic system to 2 and results in what is conventionally referred to as the energy state approximation. Note that in the application of singular perturbation theory the solution is represented by a powers series expansion in ϵ. The energy state approximation corresponds to the zeroth-order term in that expansion and is referred to, henceforth, as the reduced problem. In essence, altitude and flight-path angle dynamics are assumed fast in comparison to energy and mass dynamics, and altitude now takes on the role of a control variable.[9] The differential equations [Eqs. (27) and (28)] are reduced to algebraic equations, which yield the following relations:

$$\gamma_0 = 0 \tag{29}$$

$$L_0 = m[(\mu/r^2) - (V^2/r)] \tag{30}$$

The subscript zero denotes reduced solution values and is omitted in the following where not deemed necessary for clarity. The reduced solution Hamiltonian is given by

$$H_0 = \lambda_E \dot{E} + \lambda_m \dot{m} + \text{constraints} = 0 \tag{31}$$

where

$$\lambda_m(t_f) = -1.0 \tag{32}$$

Satisfaction of the minimum principle with respect to altitude h and rocket throttle setting η is equivalent to the following operation[7,10,11]:

$$h_0^*, \eta_0^* = \arg \max_{h,\eta} [V(T-D)/f] \Big|_{\substack{E = \text{const} \\ T > D \\ q \leq q\text{max} \quad Q \leq Q\text{max}}} \tag{33}$$

Consideration of constraints (18) and (19) simply limits the search space over which the maximization of Eq. (33) takes place. The superscript asterisk denotes an optimal value of control. This operation yields both an optimal altitude program as a function of vehicle energy and mass and the corresponding optimal rocket throttle control. The procedure proves computationally efficient and suitable for on-line implementation. However, further improvements in computational speed can be obtained.
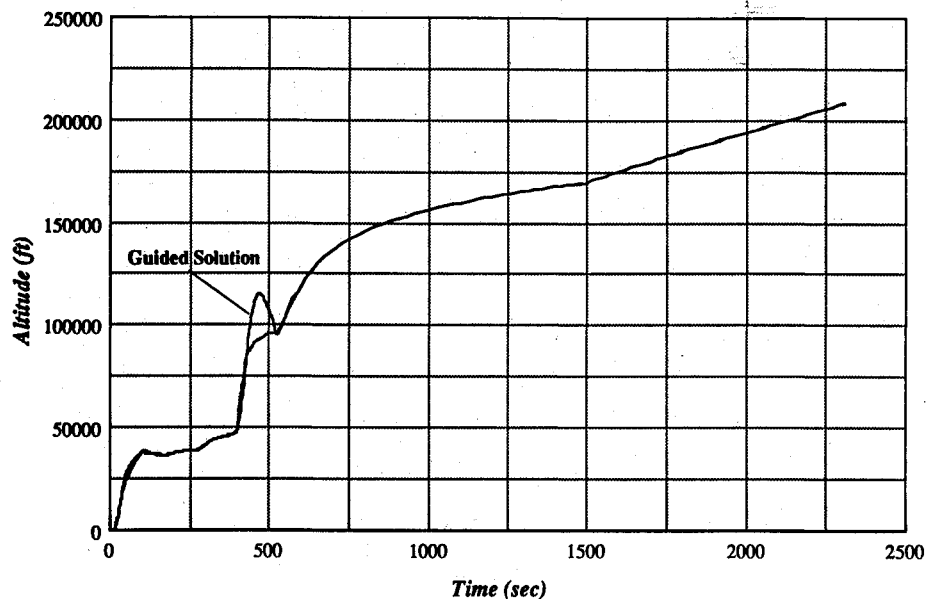

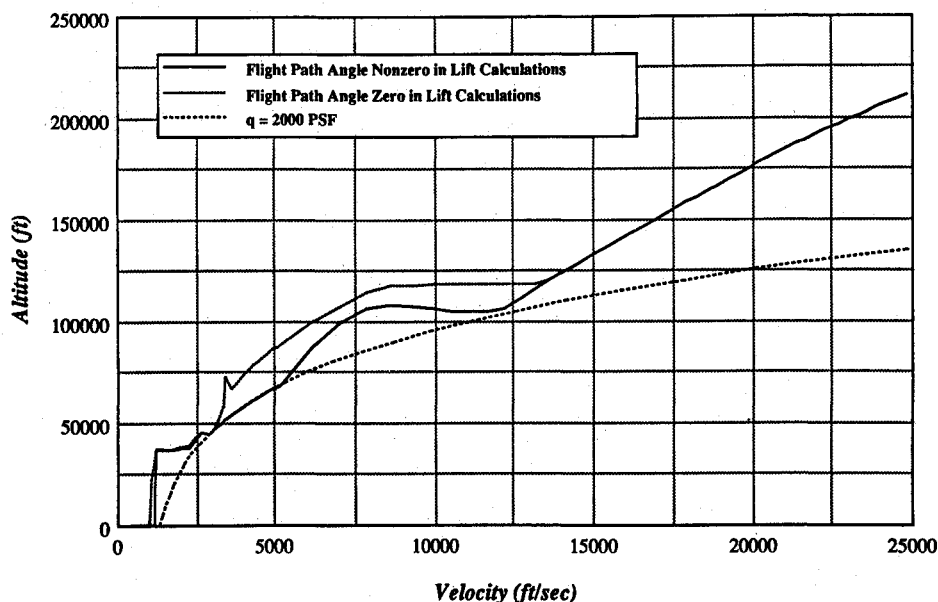Fig. 6 Comparison of the guided solution for model 3 with reduced solution.

Fig. 7 Comparison of reduced solutions for model 3 with and without compensation for flight-path angle effects.

Note that η appears linearly in the Hamiltonian. The result is a bang-bang control solution for rocket throttle setting.[12] A switching condition for rocket throttle S can be determined by evaluating $\partial H_o/\partial \eta$ and is given by

$$S = \lambda_E(V/m) - \lambda_m c_r \tag{34}$$

However, because of costate dependence, further manipulation of Eq. (34) is necessary to determine its algebraic sign. Using Eq. (31) to eliminate λ_E in Eq. (34) and taking into account the sign of λ_m yields the following analytic conditions that govern rocket throttle setting:

$$\eta = 0 \quad \text{if} \quad [(c_r - c_s)/c_r]T_s > D \tag{35a}$$

$$\eta = 1 \quad \text{if} \quad [(c_r - c_s)/c_r]T_s < D \tag{35b}$$

The influence function λ_m represents the variation in the performance index J with respect to mass.[12] Since $J = -m(t_f)$, λ_m cannot change sign (i.e., it is not possible for a reduction in vehicle mass as fuel is expended along the climb path to increase the final mass of the vehicle). The analytic test conditions (35) can be used in place of the search loop for η in Eq. (33). This substitution results in significant computational savings.

Intermediate values of rocket throttle setting (i.e., $0 < \eta < 1$) are not optimal. This fact is revealed by examination of the matrix H_{uu}, which is required to be at least positive semidefinite along an optimizing singular arc.[12] Here, the symbol u represents a general control vector. For convenience in presenting this argument, V rather than h is taken as the control-like variable, so that $u^T = [V, \eta]$. The determinant of H_{uu}, which is symmetric, must be greater than or equal to zero for positive semidefiniteness. However, it can be shown that

$$\det H_{uu} = -\{H_{V\eta}\}^2 \tag{36}$$

Thus, the determinant of H_{uu} is negative for $H_{V\eta} \neq 0$. Since $H_{V\eta}$ is nonzero in general, intermediate values of rocket throttle setting cannot be optimal.

It can happen that the velocity set is not convex in a region of interest, and, in the absence of convexity, one cannot guarantee that an optimal control exists. Thus, a test for convexity should be made, and the possibility of a chattering control solution considered. Conclusions regarding this matter are model dependent and are discussed in Ref. 13. Let it suffice to say that no chattering solutions for rocket throttle control were found for the vehicle models examined.

The reduced solution costates are not required to determine the reduced solution altitude profile and corresponding rocket throttle controls. However, they are needed in subsequent boundary layer analysis. Assuming that the heating rate constraint is independent of angle of attack, they are determined as

$$\frac{\partial H_0}{\partial \gamma} \Rightarrow \lambda_{\gamma 0} = 0, \quad \frac{d\lambda_{m_0}}{dt} = \frac{-\partial H_0}{\partial m} \Rightarrow \lambda_{m_0} \cong \frac{-m(t_f)}{m} \tag{37}$$

$$\frac{\partial H_0}{\partial L} \Rightarrow \lambda_{\gamma 0} = \lambda_{E_0}\frac{2KV^2 L_0}{qs}$$

$$H_0 = 0 \Rightarrow \lambda_{E_0} = \lambda_{m_0}\frac{fm}{V(T-D)} \tag{38}$$

where the approximation for λ_{m_0} is obtained by neglecting the contribution of induced drag in the deriviation of $d\lambda_{m_0}/dt$.[14]

General Analysis

Consider now the full model complexity formulated in Sec. II with the exception that flight remains constrained to a vertical plane. That is, consider flight over the entire Mach range, including the subsonic and supersonic regimes. Assume

a multicycle propulsion system consisting of turbojet, ramjet, scramjet, and rocket cycles (i.e., $n = 4$). Allow for a component of net thrust normal to the velocity vector and consider the possibility that the performance of one or more of the airbreathing engine cycles is dependent on vehicle angle of attack. Consider also the constraint on axial acceleration given by Eq. (20). The method for obtaining the reduced solution proceeds as before.

Setting $\epsilon = 0$ in Eqs. (1-4) reduces the differential equations (3) and (4) to algebraic relations:

$$\gamma_0 = 0 \tag{39}$$

$$L_0 = m(\mu/r^2 - V^2/r) - F_S \tag{40}$$

The reduced solution Hamiltonian is again given by Eq. (31). Satisfaction of the minimum principle with respect to h and π is equivalent to the following operation:

$$h_0^*, \pi^* = \arg \max_{h,\pi}[V(F_C - D)/f] \Big|_{\substack{E = \text{const} \quad F_C > D \\ q \le q\text{max} \quad Q \le Q\text{max} \\ n_1 \le n_{1\text{max}} \quad n_2 \le n_{2\text{max}}}} \tag{41}$$

where at each step in the search procedure, α_0 is iteratively determined to satisfy Eq. (40) at trimmed conditions. This operation yields both an optimal altitude program as a function of vehicle energy and mass and the corresponding optimum engine controls. Note that the number of nested search loops can be large, leading to a significant, though manageable, computational burden. As in the previous subsection, it is desirable to substitute analytic switching conditions for engine throttle control search loops whenever possible, thus decreasing the time required to obtain a solution.

Drag will typically be nonlinearly dependent on vehicle lift L_0. Unlike in the previous subsection, L_0 now depends on engine controls through F_S, as given in Eq. (11). Thus, the φ_i and the η_j both enter nonlinearly in the Hamiltonian. If we neglect the dependence of reduced solution drag on the sine component of net thrust F_S, then the η_j enter linearly in H_0. In such case, we have bang-bang solutions for the η_j with possible singular arcs along which intermediate throttle settings may be optimal. The switching functions are determined as before from $\partial H_0/\partial \eta_j$. Following the elimination of costate dependence, they are given by

$$S_j = \{f(\pi) \cos(\alpha + \epsilon_{Tj})/[F_C(\pi) - D]\} - c_j$$

$$j = 1 + n \text{ to } p \tag{42}$$

Throttle settings are then governed by the following relations:

$$\eta_j = 0 \quad \text{if} \quad S_j < 0 \tag{43a}$$

$$\eta_j \text{ singular} \quad \text{if} \quad S_j = 0 \text{ for finite time} \tag{43b}$$

$$\eta_j = 1 \quad \text{if} \quad S_j > 0 \tag{43c}$$

The S_j are dependent on the $\eta_k, k \neq j$. Thus, an iterative procedure is required to arrive at the optimal combination of throttle settings if $j > 1$. When appropriate, conditions (43) are used to eliminate one or more of the search loops in Eq. (41).

Switching Conditions for Mutually Exclusive Cycle Operations

Thus far in the analysis, it has been assumed that each engine cycle can be independently controlled. Since much of the captured mass flow and some or all of the engine hardware will be shared by the various engine cycles employed, it is perhaps useful to consider operation of the various airbreathing cycles as mutually exclusive.

One can view the case of mutually exclusive engine cycles as a problem in which the system equations are discontinuous at

cycle transition points along the trajectory. Following the terminology of Ref. 12, suppose that one set of system equations,

$$\dot{x} = f^{(1)}(x,u,t) \tag{44}$$

applies for $t < t_1$, where t_1 is free, and another set of system equations applies for $t > t_1$, namely

$$\dot{x} = f^{(2)}(x,u,t) \tag{45}$$

Here, x and u denote general state and control vectors, respectively. It is necessary for optimality that

$$H^{(1)}(t_1 -) = H^{(2)}(t_1 +) \tag{46}$$

Condition (46) can be used to determine the optimal point of transition from one set of system equations to another. In this case, $f^{(1)}$ and $f^{(2)}$ differ only by the maximum thrust produced by the particular engine cycle being employed and by the associated difference in fuel consumption. Satisfaction of Eq. (46) can be reduced to the following equality where the condition $H_0 = 0$ has been employed to eliminate costate dependence

$$\frac{[T_i \cos(\alpha + \epsilon_{T_i}) - D]}{c_i T_i} = \frac{[T_j \cos(\alpha + \epsilon_{T_j}) - D]}{c_j T_j} \tag{47}$$

This result is, in fact, obvious from examination of Eq. (41). That is to say, points at which a change in engine cycle can occur require that the function to be maximized be equal for either choice of the propulsion cycle. When the functional evaluations are not equivalent, one or the other is greater and dictates the optimal choice of cycle. In reality, dual cycle combustion over a finite range of Mach number will likely be required to smoothly transition from one engine type to another.[15]

Bank Angle as a Control

It is reasonable to assume that the performance of scramjet engines will be sensitive to vehicle angle of attack. Furthermore, it is quite likely that thrust production will depend on angle of attack in a nonlinear way. Given that this is true, any particular engine installation will exhibit an angle of attack for which engine performance is best. This angle of attack for best engine performance, call it the design angle of attack, may in turn vary with Mach number.[16] If such nonlinear behavior is assumed and the optimal flight path is constructed using Eq. (41), one finds that, since fuel optimization is very sensitive to engine performance, the optimal trajectory tends to remain on a contour along which the design angle of attack is maintained.

It has been suggested that various design constraints could lead to a vehicle configuration for which overall performance is improved in a given Mach regime if the design angle of attack is maintained while flying at lower altitudes and, hence, at higher values of dynamic pressure. Of course, maintaining the design angle of attack at a higher dynamic pressure generates additional lift. This additional lift causes the vehicle to immediately climb above the desired flight path. Thus, in order to fly along such a path, the extra lift associated with maintaining the design angle of attack must be eliminated. One procedure suggested for accomplishing this task is to roll back and forth in such a way that, on average, the component of lift in the vertical direction is reduced to that required to maintain the optimal climb rate. It could be more practical to appropriately offset the initial vehicle heading and to then execute a single coordinated turn that accomplishes the same objective. However, flexibility in compensating for errors would then be reduced. Bank angle was introduced as an optional control variable in order to allow designers to use this algorithm to investigate and trade between the increased com-

plexity of variable geometry engines that can alter the design angle of attack as needed and fixed geometry installations that lack such freedom.

With bank angle thus introduced, satisfaction of the minimum principle with respect to h, π, and α is equivalent to the following operation:

$$h_0^*, \pi^*, \alpha_0^* = \arg \max_{h,\pi,\alpha} [V(F_C - D)/f] \Big|_{\substack{E = \text{const} \quad F_C > D \\ q \le q\text{max} \quad Q \le Q\text{max} \\ n_1 \le n_{1\text{max}} \quad n_2 \le n_{2\text{max}}}} \tag{48}$$

where bank angle σ is determined so that

$$L \cos\sigma = L_0 \tag{49}$$

IV. Boundary-Layer Analysis: Feedback Guidance Laws

The unconstrained, zeroth-order, initial boundary-layer solution associated with Eqs. (1–4) is obtained by introducing the time transformation $\tau = t/\epsilon$ and again setting $\epsilon = 0$. That is, energy and mass are held constant while altitude and flight-path angle dynamics are examined on a stretched time scale. The resulting necessary conditions for optimality yield an optimal feedback guidance law for lift control that depends on the unknown costate λ_γ. In the absence of a state inequality constraint such as Eq. (18), the reduced solution serves as an equilibrium point for the boundary-layer dynamics. In such case, a suitable approximation to λ_γ can be obtained by linearizing the boundary-layer necessary conditions about the reduced solution.[17] However, for energy levels where the reduced solution lies on the state constraint boundary, the reduced solution may no longer serve as an equilibrium point. In fact, the theory for applying singular perturbation analysis to problems with state inequality constraints is not yet fully developed. Reference 18 examines the major issues that must be addressed in developing the theory. It is noted that the boundary-layer dynamics are of finite duration on the fast time scale for many problems of practical interest. Two possible solution methodologies are also presented. However, in this section, we examine an effective suboptimal approach for treating the boundary-layer altitude and flight-path angle dynamics. The boundary-layer control solution for engine throttle settings are similar to those of the reduced solution. The η_j enter the Hamiltonian linearly, but the switching conditions that govern their behavior are also dependent on the unknown costate λ_γ. This dependence drops out of the switching conditions if the sine component of thrust F_S is neglected, yielding conditions (42) and (43).

Feedback Linearization

As an alternative approach to handling the control of altitude and flight-path dynamics, a nonlinear transformation (NLT) technique, sometimes referred to as feedback linearization, can be employed as follows.[13] Consider first the boundary-layer altitude and flight-path angle dynamics given in Eqs. (27) and (28) on the transformed time scale $\tau = t/\epsilon$. Take successive total time τ derivatives of r until explicit dependence on the control appears:

$$\frac{d^2 r}{d\tau^2} = \frac{L}{m} \cos\gamma + \frac{V^2}{r} \cos^2\gamma - \frac{\mu}{r^2} \tag{50}$$

The control L appears in the second time derivative and we define U, the pseudocontrol, as

$$U \equiv \frac{d^2 r}{d\tau^2} \tag{51}$$

It is desired that U be determined as follows:

$$U = K_p(r_0 - r) + K_d\left(\frac{dr_0}{dt} - \frac{dr}{d\tau}\right) \tag{52}$$

where r_0 denotes the reduced solution radius at the current energy level, and the time derivative of r_0 denotes the climb rate required to stay on the reduced solution climb path as energy is gained. This climb rate can be estimated by defining an appropriate increment in energy, evaluating the reduced solution at this higher energy level, and then estimating the required climb rate using a forwards difference.

The inverse transformation is defined by solving for L in Eq. (51) using Eqs. (50) and (52),

$$L = [U + \mu/r^2 - (V^2/r)\cos^2\gamma]m/\cos\gamma \qquad (53)$$

This lift control solution is constrained directly by Eq. (21). Note that, as r and γ approach their reduced solution values, Eq. (53) approaches the reduced solution value of lift given by Eq. (30). Taking the Laplace transform of Eqs. (51) and (52), it can be seen that the transformed system is mathematically equivalent to a linear system whose closed-loop transfer function is given by

$$G(s) = (K_d s + K_p)/(s^2 + K_d s + K_p) \qquad (54)$$

The gains K_p and K_d for the second-order system can be written in terms of the damping ratio ζ and natural frequency ω_n as

$$K_p = \omega_n^2, \qquad K_d = 2\zeta\omega_n \qquad (55)$$

The performance of this controller can be dictated by selecting the values of K_p and K_d to yield the desired dynamic response. This lift control solution applies equally well to the unconstrained or the state inequality constrained case.

Direct extension of the lift control solution presented earlier to include the angle-of-attack effects included in Eqs. (1–4) results in the following feedback control law:

$$\alpha^* = \left\{ \alpha : \left[U + \mu/r^2 - (V^2/r)\cos^2\gamma \right](m/\cos\gamma) - (F_S + L) = 0 \right\} \qquad (56)$$

The pseudocontrol U is again defined by Eq. (52) and as before the proportional gain K_p and the rate gain K_d are selected to yield the desired controller performance. The application of this technique for a general class of aerospace plane tracking problems is discussed in Ref. 19.

V. Numerical Results

Vehicle Models

Three different vehicle models were employed to generate the numerical results presented in this section. The first, referred to as model 1, is based on a hypersonic research vehicle concept studied by NASA in the 1970s and is powered by a combination of scramjet and rocket propulsion.[14] This model is useful only in the hypersonic regime. The second model is based on a general hypersonic aerodynamic model example (GHAME) developed more recently by NASA.[20] A nominal configuration of 233.4-ft total length and 300,000-lb gross takeoff weight was assumed. The trimmed aerodynamic characteristics were taken directly from the GHAME II documentation (where II refers to the data set generated via the hypersonic arbitrary body program, not the original data set assembled using experimental data) and extend from takeoff to orbital velocities. Thrust is provided by a multicycle propulsion system composed of turbojet, ramjet, scramjet, and rocket engines. The airbreathing propulsive characteristics were adopted from Ref. 21. A rocket, sized for orbital insertion (roughly 15,000 lb of thrust in vacuum), is assumed available over the entire Mach range. Because of the simplicity of this engine data, this system corresponds to the case $p = n = 4$ in Eqs. (10), (11), and (15). As a result, the switching conditions given by Eqs. (43) can be used to determine all of the cycle transition points. Figure 2 presents the adopted variation

in fuel specific impulse with Mach number for the various engine cycles. A third model was constructed by combining an aerodynamic data set provided by NASA Langley Research Center (referred to as the Langley Accelerator) with the propulsive data described earlier. Additional details regarding these models are available in Ref. 11.

Note the limitations of these vehicle models. The various engines were roughly sized by trial and error. The combinations of engine and airframe data do not represent properly integrated configurations. The generation of scramjet thrust due to mass ejection when operating above a stoichiometric fuel-to-air ratio is not modeled. Thrust induced pitching moments, which can be significant,[13] were not considered when trimming the aircraft.

A simple model for convective heating rate per unit area Q was adopted from Ref. 22:

$$Q = (4.919E\text{-}08)\,\rho^{0.5}\,V^{3.0} \qquad (57)$$

Equation (57) gives Q in W/cm^2 given density in kg/m^3 and velocity in m/s and corresponds to equilibrium conditions on the surface of a sphere or wing leading edge 10 cm in radius and cooled by reradiation alone. For reference, a contour of $Q = 800$ W/cm^2 in the altitude-velocity plane corresponds roughly to a contour along which skin temperature remains at approximately 2000°F, 3 ft aft of the leading edge assuming laminar flow.[23]

Reduced Solution: Simplified Analysis

Reduced solution trajectories were first generated by carrying out the maximization process indicated in Eq. (33) over an energy range corresponding to $V = 5000$ ft/s at $h = 0$ to $V = 25,000$ ft/s at $h = 200,000$ ft. Figure 3 depicts a set of reduced solution trajectories for model 1 in the altitude-velocity plane. Dynamic pressure is limited to 2000 psf, whereas maximum allowable heating rate is varied. The trajectories follow the dynamic pressure constraint boundary until the specified contour of maximum heating rate is encountered. The paths then follow the specified constant heating rate contour until reaching the trajectory for which no heating rate constraint was enforced. At this point, the heating constraint becomes inactive and the trajectory rejoins approximately the unconstrained climb path. The performance penalty paid in enforcing the heating constraint is presented in Fig. 3 as both time required and percent gross weight consumed to achieve an orbital energy level. This performance penalty must be weighted against the complications of using active cooling, the weight of heat shielding, and various other factors in the vehicle design process.

The mechanism causing the altitude discontinuity at a velocity of 22,000 ft/s is discussed in Ref. 17 and is similar to that which has been noted in the transonic region for supersonic fighter aircraft.[7] Included in Fig. 3 is the rocket switching surface, i.e., the contour along which the switching function [Eq. (34)] remains zero. At altitudes below this contour, the optimal rocket throttle setting is zero, whereas above the contour, the optimal throttle setting is one.

Reduced Solution: General Analysis

Computational investigations of the sensitivity of scramjet performance to changes in angle of attack predict highly nonlinear behavior.[16] Figure 4 presents a scramjet thrust scaling factor employed to model this effect. This figure is based on a liberal interpretation of the computational results presented in Ref. 16. This curve is shifted with respect to the horizontal axis in order to represent inlet designs that favor maximum engine performance at an angle of attack other than zero.

Figure 5 presents variations in the dynamic pressure constrained reduced solution trajectories for model 2 generated by carrying out the maximization process indicated in Eq. (41) over the energy range from takeoff to orbit. No heating rate or acceleration limits are enforced. Thrust variation with angle of

attack for both the ramjets and scramjets, as depicted in Fig. 4, is included. The angle of attack for best engine performance is varied over the range from 0.5 to 3.0 deg. The horizontal bars indicate the velocity range over which the operation of each engine cycle was deemed optimal, including regions of cycle overlap. When only scramjets are operating, the vehicle tends to prefer a path along which the design angle of attack is strictly maintained. As a result, significant variation in the optimal altitude profile is evident. The performance penalty paid for a change in the design angle of attack was determined to be modest, since in this Mach region, the acceleration capability of the vehicle is high. However, the corresponding variation in heat load could lead to significant changes in the design weights of vehicle heat shield and heat load management hardware, directly impacting payload delivered to orbit. When the thrust scaling factor of Fig. 4 is assumed Mach dependent in accordance with the results of Ref. 16, further variation in the trajectory is experienced.[11]

The peak in the trajectories at approximately 3000 ft/s in Fig. 5 is due to turbojet shutdown. This peak is significantly reduced when the turbojet inlet area is increased, indicating that the climb away from the dynamic pressure constraint boundary is due to the decreasing level of thrust available from the turbojet as the Mach number increases. With an increase in altitude comes a reduction in vehicle drag. The turbojet switching surface is encountered at an altitude of approximately 75,000 ft and the turbojet is shut down. The SCRAMJET almost immediately switches on and, with a much greater magnitude of thrust, can sufficiently overcome vehicle drag, even at a higher dynamic pressure. Thus, the trajectory returns to the dynamic pressure constraint boundary. Note that the ramjet is turned on at a very low Mach number (i.e., $M = 0.81$) even though it is extremely inefficient in this speed range (see Fig. 2). This behavior has been noted by past researchers and is due to the presence of a pinch point (i.e., a point of minimum thrust minus drag) in the transonic region. The size of the ramjet was selected without regard to its weight. However, optimization of the vehicle configuration must take into account the mass of each engine installation. Results obtained indicate that the optimal trajectory for such an optimized configuration may prefer the use of rocket (rather than ramjet) thrust to augment turbojet thrust at the transonic pinch point.[11]

As stated earlier, cycle operations are represented in Fig. 5 by horizontal bars. The transition points were found to be very nearly the same for thrust independent of, or dependent on, angle of attack. The overlap in airbreathing cycles is, in fact, desirable to provide smooth cycle transitions. For model 2, turbojet sizing requires about 25 ft² of inlet area, whereas the total number of ramjet modules selected require 200 ft² of inlet area. Thus, it should be possible to start the majority of the ramjet engines in a sequence that avoids excessive accelerations while maintaining turbojet thrust. Once the velocity for turbojet shutdown is reached, turbojet airflow can be diverted to the remaining ramjet modules. The number of required scramjet modules is likewise larger than the number of required ramjet modules, and a similar argument for cycle overlap can be made. Of course, the actual system will no doubt share much of the engine hardware among the various cycles employed in addition to sharing the captured mass flow. Thus, the actual optimization of engine transitions will be more complex.

Reduced Solution: Optional Use of Bank Angle Control

Modulation of the vertical component of lift via bank angle variation was also evaluated for model 2. Carrying out the maximization process indicated in Eq. (48) alters the trajectories presented in Fig. 5 only slightly. The changes correspond to those portions of the trajectory where $\alpha_0 < \alpha_{design}$. As such, only a very modest gain in performance was achieved. However, if design constraints were to force the scramjet design

angle of attack to differ significantly from the angle of attack for zero lift, much greater savings could be obtained.

Near Optimality of the Reduced Solution Climb Path

The validity of the time scale decomposition artificially introduced into Eqs. (1–4) was assessed in Ref. 19 by a direct comparison of a reduced solution climb path to the optimal trajectory of the system [Eqs. (1–4)] with $\epsilon = 1$. Excellent agreement between the two trajectories was obtained except in the terminal phase, which must be treated with a terminal boundary-layer correction. The terminal boundary-layer problem of injection into orbit is not treated in this paper.

Simulation of Guided Flight

Figure 6 depicts the altitude time history for simulated flight of model 3 using the derived lift control law [Eq. (53)] to track its corresponding reduced solution. The ramjet cycle was eliminated and the trajectory is subject to the following constraints: dynamic pressure ≤ 2000 psf, reference heating rate ≤ 400 W/cm², and axial acceleration ≤ 3.0 g. In general, this vehicle preferred to climb in order to satisfy an axial acceleration limit rather than to throttle back the engines. The rapid climb at roughly 400 s is due to scramjet turn on and this preferred behavior. The large overshoot at just before 500 s is due to the inability of the vehicle to pull down rapidly enough as the altitude for which $n_1 \leq 3$ at full throttle is approached. This overshoot can be reduced somewhat by careful gain scheduling and having the controller look ahead in energy. However, the need to fine tune the controller for each trajectory generated is not desirable for the intended applications of this algorithm. This problem has less to do with the controller than with the generation of the trajectory itself.

Over the vast majority of the trajectory, the flight-path angle is small and the flight-path angle rate very modest, so that Eq. (40) provides a good approximation to the actual lift required to follow the flight trajectory. However, when the scramjet is initially turned on at a relatively high value of dynamic pressure, the energy rate of the vehicle is greatly increased. The necessity of simultaneously climbing to avoid violating the dynamic pressure constraint boundary results in a large flight-path angle rate. For this reason, the time scale separation assumed in Eqs. (1–4) is simply not appropriate over this small portion of the trajectory. A simple correction procedure can be applied when generating the reduced solution climb path to eliminate this problem.

Reduced Solution Correction Procedure

The correction just alluded to consists of estimating the flight-path angle along the reduced solution climb path and estimating the time of flight between selected energy levels. These estimates are then combined to form an estimate of the flight-path angle rate. Relation (3) is then inverted to obtain the value of lift that will have to be commanded to follow the reduced solution climb path. By restricting acceleration normal to the flight path (i.e., limiting lift) as the reduced solution is constructed, a feasible trajectory is always obtained.

Figure 7 depicts the reduced solution climb path for model 3 again with a maximum dynamic pressure of 2000 psf, a maximum aerodynamic heating rate of 400 W/cm², but with a maximum axial acceleration of 1 g to amplify the problem discussed earlier. In particular, $\gamma = 0$ in the lift calculations. Also depicted is the modified trajectory when the correction method described earlier is implemented (γ and $d\gamma/dt \neq 0$). The results are quite dramatic over the speed range from 3000 to 12,000 ft/s when depicted in the altitude/velocity plane. The near vertical altitude transition at a velocity of approximately 3000 ft/s is eliminated, as is the dive that followed. The arc that follows in the velocity range from 5000 to 13,000 ft/s corresponds to the region over which the axial acceleration limit is active. Less altitude change is commanded in this region; the engines are instead throttled back to reduce the

axial acceleration. The remainder of the trajectory, the same for either case, constitutes flight along the heating constraint boundary. Despite the significant change in trajectory, only 200 additional pounds of fuel are consumed and the difference in time of flight is only about 60 s. These small differences are due to the fact that the velocity interval from 3000 to 12,000 ft/s is traversed very rapidly in time, corresponding to only a small fraction of the total time of flight.

VI. Conclusions

This paper has identified a number of the modeling and analysis issues associated with single-stage-to-orbit airbreathing vehicles, real-time ascent trajectory optimization, and the formulation of suitable guidance laws. In particular, an energy state approximation was shown to be useful for rapid trajectory generation. Assumptions regarding propulsion system characterstics, namely, that they enter into the optimization problem in a linear fashion, allow one to determine the optimal engine transition points as a function of state using a simple iterative test, providing further improvement in computational speed. Functional dependence of scramjet thrust on vehicle angle of attack has a major impact on the nature of fuel-optimal ascent trajectories. The derived algorithm can be extended to investigate impact of roll maneuvers on the index of performance. Over those limited regions of flight where the energy state approximation proves inadequate, simple lift corrections that account for nonzero flight-path angle and flight-path angle rate significantly improve the trajectory generation methodology. Other researchers' comparison of a trajectory generated with the reduced-order algorithm presented in this paper to the full-order optimal trajectory showed excellent agreement. Finally, feedback linearization can be applied on the stretched boundary-layer time scale and yields an effective lift control solution useful for vehicle guidance.

References

[1]Heppenhiemer, T. A., "Keepers of the Flame," *Air & Space/ Smithsonian,* Vol. 4, No. 5, 1989-90, pp. 88–95.

[2]"National Aero-Space Plane, A Technology Development and Demonstration Program to Build the X-30," U.S. General Accounting Office Report to Congressional Committees, GAO/SNIAD-88-122, April 1988.

[3]Williams, R. M., "National Aero-Space Plane: Technology for America's Future," *Aerospace America,* Vol. 24, No. 11, 1986, pp. 18–22.

[4]Gregory, T. J., "Credibility of NASP," *Aerospace America,* Vol. 27, No. 9, 1989, pp. 42–46.

[5]Hardtla, J. W., Piehler, M. J., and Bradt, J. E., "Guidance Requirements for Future Launch Vehicles," AIAA Paper 85-2462, Aug. 1985.

[6]Bradt, J. E., Hardtla, J. W., and Cramer, E. J., "An Adaptive Guidance Algorithm for Aerospace Vehicles," AIAA Paper 85-1917, Aug. 1985.

[7]Bryson, A. E., Jr., "Energy-State Approximation in Performance Optimization of Supersonic Aircraft," *Journal of Aircraft,* Vol. 6, No. 6, 1969, pp. 481–488.

[8]Kelley, H. J., "Flight Path Optimization with Multiple Time Scales," *Journal of Aircraft,* Vol. 8, No. 4, 1971, pp. 238–240.

[9]Calise, A. J., "Extended Energy Management Methods for Flight Performance Optimization," *AIAA Journal,* Vol. 15, No. 3, 1977, pp. 314–321.

[10]Calise, A. J., and Prasad, J. V. R., "Pulse Motor Control for Maximizing Average Velocity," *Journal of Guidance, Control, and Dynamics,* Vol. 12, No. 2, 1989, pp. 169–174.

[11]Corban, J. E., "Real-Time Guidance and Propulsion Control for Single-State-to-Orbit Airbreathing Vehicles," Ph.D. Dissertation, Georgia Inst. of Technology, Atlanta, GA, Dec. 1989.

[12]Bryson, A. E., Jr., and Ho, Y. C., *Applied Optimal Control,* Hemisphere, New York, 1975.

[13]Corban, J. E., Calise, A. J., and Flandro, G. A., "Optimal Guidance and Propulsion Control for Transatmospheric Vehicles," AIAA Paper 89-3617, Aug. 1989.

[14]Calise, A. J., Corban, J. E., and Flandro, G. A., "Trajectory Optimization and Guidance Law Development for National Aerospace Plane Applications," *Proceedings of the 1988 American Control Conference,* Vol. 2, 1988, pp. 1406–1411.

[15]Kandebo, S. W., "Pratt Demonstrates Low-Speed Propulsion Concept for National Aero-Space Plane," *Aviation Week & Space Technology,* June 26, 1989, p. 79.

[16]Walton, J., "Performance Sensitivity of Hypersonic Vehicles to Changes in Angle of Attack and Dynamic Pressure," AIAA Paper 89-2463, 1989.

[17]Corban, J. E., Calise, A. J., and Flandro, G. A., "Trajectory Optimization and Guidance Law Development for Transatmospheric Vehicles," *Proceedings of the 1989 IEEE International Conference on Control and Applications,* Institute of Electrical and Electronics Engineers, New York, 1989.

[18]Calise, A. J., and Corban, J. E., "Optimal Control of Singularly Perturbed Nonlinear Systems with State-Variable Inequality Constraints," *Journal of Guidance, Control, and Dynamics* (to be published).

[19]Van Buren, M. A., and Mease, K. D., "Aerospace Plane Guidance Using Geometric Control Theory," *Proceedings of the 1990 American Control Conference,* Vol. 2, 1990, p. 1829–1838.

[20]Bowers, A. H., and Iliff, K. W., "A Generic Hypersonic Aerodynamic Model Example (GHAME) for Computer Simulation," Proposed NASA Technical Note, Ames Research Center, June 1988.

[21]Waltrup, P. J., Anderson, G. Y., and Stull, F. D., "Supersonic Combustion Ramjet (SCRAMJET) Engine Development in the United States," Third International Symposium on Air Breathing Engines, Paper 76-042, March 1976.

[22]Tauber, M. E., Menees, G. P., and Adelman, H. G., "Aerothermodynamics of Transatmospheric Vehicles," AIAA Paper 86-1257, June 1986.

[23]Johnston, P. J., Whitehead, A. H., Jr., and Chapman, G. T., "Fitting Aerodynamics and Propulsion into the Puzzle," *Aerospace America,* Vol. 25, No. 9, 1987, pp. 32–37, 42.